NASA Technical Memorandum 102608

THE UTILIZATION OF AN INFRARED IMAGING SYSTEM AS A COOLING SLOT BLOCKAGE DETECTOR IN THE INSPECTION OF A TRANSPIRATION COOLED NOZZLE

STEPHEN E. BORG, ROBERT E. WRIGHT, JR., DAVID W. ALDERFER, AND JANET C. WHIPPLE

JANUARY 1990

National Aeronautics and Space Administration

Langley Research Center
Hampton, Virginia 23665-5225

ABSTRACT

A comprehensive examination of the 8-foot high temperature tunnel's transpiration-cooled nozzle was completed using an infrared imaging radiometer to locate regions of cooling flow irregularities characterized by obstruction of three or more adjacent cooling slots. Restrictions in the cooling flow were found and cataloged. Those blockages were due primarily to the presence of residual phosphoric acid being discharged from some of the cooling slots. This acid was used during construction of the nozzle components and was to have been purged prior to its delivery to the NASA Langley Research Center (LaRC). In addition, a radial displacement of one section of discs located in the spool piece was inspected and cataloged for future reference. There did not seem to be a serious restriction of flow in this defect, but infrared images indicated reduced slot activity within the gouge. The radiometer survey uncovered regions where closer inspection is recommended but did not cover the entire surface area of the three nozzle subsections due to equipment limitations. A list of areas with suspected problems is included in Appendix A.

INTRODUCTION

The transpiration cooling of a structure is a technique used to moderate surface temperatures in regions of high thermal loading. This reduction in wall temperature reduces the probability of failure due to the effects of localized overheating. A transpiration cooled structure is essentially a porous object. A fluid, typically air, is passed through surface pores of the object and injected into the high-temperature flow. This forms an artificial boundary layer which insulates the surface from the heating effects of the flow. The injected fluid also provides additional cooling to the internal structure of the device through a form of forced convection.

Restrictions to a significant number of cooling slots could seriously jeopardize the ability of the nozzle to maintain a safe wall temperature during operating conditions. It had been calculated that a restriction of three or more adjacent slot rings could result in excessively high nozzle surface temperatures under normal operating conditions. The effects of localized overheating could reduce the expected service lifetime of the nozzle as well as pose an increased risk to personnel nearby.

In an effort to guarantee the passage of air through the slots, the manufacturer had the cooling passages of the nozzle flushed with a cleansing solution of phosphoric acid during construction. A soap bubble test with pressurized air was performed to verify that there was flow within the cooling slots. A residual film of soap and phosphoric acid within a nozzle section could significantly reduce the volume of cooling flow to a critical area of the nozzle. Particles and debris that became lodged in the passages during shipment could also pose a significant threat to the long term-reliability of the transpiration cooled nozzle.

The interior surface of the transpiration-cooled nozzle was inspected prior to its installation in the 8' High Temperature Tunnel (HTT). This was necessary in order to verify that sufficient cooling flow rates were within each nozzle section and possible nonfunctioning slots were located. Infrared imaging had been selected as the inspection method for detecting blockages in the cooling passages of the nozzle since it can cover relatively large surface areas quickly and provide quantitative data for later study. Blockages were determined by measuring the temperature of individual slots with an infrared imager as heated gas was passed through them.

The actual inspection of the nozzle was performed by an infrared imager working in conjunction with a multiaxis positioning system. As heated and filtered air was pumped through the cooling slots, the interior surface was circumferentially scanned by the imager along the centerline axis of the nozzle. This scanning algorithm was capable of providing a complete temperature history of the nozzle's interior surface. The images collected from each nozzle subsection were cataloged and stored on video tape for postprocessing.

HISTORY

The infrared inspection of a transpiration-cooled structure was first demonstrated in October 1986 on a diffusion bonding test specimen supplied by the manufacturer. The test specimen was fabricated to study the effects of diffusion bonding on the ability of the slots to pass cooling air. The test specimen had surface cooling slots in the same width range as found on the nozzle (0.0025-0.008 inches).

The imager used in the feasibility test, AGA model 750, was positioned so that the slots could be viewed normal to the target surface as a test gas was passed through the slots. Cooling slot restrictions were simulated by inserting loops of bare wire and shim stock into the slots beneath the surface. This simulation reduced the slot cross sectional area by about 80 percent.

In the demonstration of the technique, it was found that the greatest slot/background resolution was obtained when air was supplied to the specimen at a temperature about 77 ^{o}F above ambient. The

infrared radiometer was able to distinguish blocked slots from unblocked slots when operated at magnifications sufficient to view individual slots. Regions with groups of three or more slots were also visible to the imager when compared to areas containing unrestricted slots. It was also noted that shielding of the target area from stray radiation sources would be necessary since highly specular reflections were observed during the test. Results from the feasibility study can be seen in Appendix B.

EXPERIMENTAL PROCEDURE

The inspection of the transpiration-cooled nozzle was carried out with an AGEMA model 880 infrared imager. The imager detects slot blockages by observing temperature variations within the cooling slots of the nozzle as heated and pressurized air is passed through them (fig. 1). The test nozzle was divided into three individual sections which were referred to as "spool piece," "approach section," and "sonic throat." In addition, the inspection was intended to reveal areas in which radial displacement of the diffusion bonded disc stacks had occurred and its effect on local flow characteristics.

The detector used in the imager is sensitive to the 8 to 12 micrometer region of the infrared spectrum. The imager generates a thermal picture by scanning the infrared radiation emitted by the target with a rotating mirror. This scan generates an instantaneous image on a mercury cadmium telluride (HgCdTe) detector. The detector processes this incident thermal energy into a synchronized analog video signal which is then digitized into either a false color or monochromatic image on a remote monitor. This imaging system generates 25 fields per second which corresponds to a framing rate of 6.25 frames per second of real-time information.

In order to develop a successful procedure for the inspection of the transpiration cooled structure, certain requirements had to be fulfilled; (1) The procedure should incorporate an efficient algorithm capable of scanning the interior quickly with a high degree of repeatability; (2) The inspection system should display the coordinates of the image data obtained at each location. Explicit knowledge of an area's location would reduce the complexity of reinvestigation should the need arise. Additionally, the inspection system must be able to inspect the varying surfaces of the individual sections without major modification. This is important since the internal diameters of the nozzle ranged from a minimum of 5.6 inches to a maximum of 36.0 inches.

As a result, the following procedure was developed. It was evident that the complexity of mapping the internal surface of the nozzle could be reduced by taking advantage of the geometrical symmetry of the interior surface. A rotating mirror mounted on a translating stage was inserted in the nozzle and traversed at regular intervals along the centerline of the nozzle specimen. An infrared imager was simultaneously mounted on another translating stage and positioned so that it was viewing the mirror along the same centerline axis (fig. 2).

The translating stages were placed on a pair of height-adjustable tables and were positioned at opposite ends of the nozzle section. A helium-neon laser was mounted to the imager's camera track and positioned so that the laser beam coincided with the optical centerline of the AGEMA 880 imager. A pair of crosshair sights, mounted at the nozzle ends, were used to define the geometrical centerline of the test specimen. The adjustable tables supporting the imager/translator and the mirror/rotator/translator were then positioned so that both the optical and geometrical axes were in complete alignment. Failure to locate the centerline of the test specimen accurately would have induced small changes in the optical pathlength during rotation of the mirror. Small changes in the optical pathlength would have periodically moved the target surface out of focus since the depth of field was less than 1.57 inches at the minimum focal distance of the 7 degree field of view lens.

Once the optical axes of the imager and mirror translation stages were aligned with the centerline of the nozzle, the imaging/positioning system was used to map the interior of the test specimen. A programmable position controller was used to maneuver the positioning devices. The method of data acquisition is specified below: The imager, fixed to a translating stage, viewed the nozzle surface via a mirror located at the opposite end of the test specimen. The mirror was mounted on a rotating stage which could then be advanced along the axis of the specimen with another translating positioner. The mirror, starting at a fixed axial position, would begin rotation in fixed angular steps around a 360 degree circle. This scanning technique would permit direct identification of a region through corresponding axial and angular coordinates. The mirror would pause between angular steps in order to obtain a minimum of 16 frames of data. These frames would be averaged later to improve the signal/noise ratio of the data. At the completion of a 360 degree ring, the mirror would then translate axially a fixed distance along the interior of the nozzle to the next location and the imager repositioned for best focus. Data obtained in this manner would be comprised of a series of sequential rings located at discrete axial distances along the centerline of the test specimen. A coordinate system for each nozzle section complete with station locations and area titles can be seen in figure 3.

The results of each scan could be viewed in real time on a color monitor and simultaneously stored on video tape for postprocessing by the software package CATS (Computer Aided Thermography Software) included with the PC-based thermal image computer system (TIC-8000). Additional postprocessing with CATS was necessary to reduce the effects of noise and other transient phenomena. The capabilities of the CATS program include thermal mapping, histograms, spot temperatures, and temperature profiles.

Precise motion control of a three degree of freedom system was not within the capabilities of the current positioning system. This led to the development of a device which would allow the two-axis positioner to control three independent axes. This was accomplished by having one

of the positioner's output ports control either of two positioning devices through a gated switch-type mechanism. Inserting this switchbox in series with one of the output ports would allow signals to be routed to either device depending upon the position of an electronically triggered multipole double throw switch (fig. 4). The switchbox could be controlled by the position controller through a 15 pin communication line or by the user through the manual operation of panel mounted switches. Further details on the design and operation of the switchbox are given in Appendix C. Figure 5 shows a circuit diagram of the switchbox.

RESULTS AND CONCLUSIONS

All experimental data were recorded on video tape at 25 fields per second with a 4 to 1 field/frame interlace. Six hundred and sixty five composite images were generated from the frame averaging of at least 16 frames of video taped data.

Manipulation of the composite images to improve resolution was attempted with a pair of high and low-pass filters. High-pass filtration improves the slot contrast while low-pass filtration removes the effects of the slots. The low-pass filtered image was then frame subtracted from the high-pass filtered image to eliminate the reflected "average" of the radiation from the image. These resulting images were processed further with Sobel edge detection filter matrices in order to emphasize the slots further (ref. 5). A miscalculation in the spatial field of view would result in some areas not being represented in the final composite images. However, the interior surface of each nozzle section was fully examined with the imager by continuously scanning between dwell points.

The inspection of the individual nozzle subsections yielded the following results. After subjecting each nozzle subsection to pressurized air ranging in temperature from 80 ^{o}F to 150 ^{o}F, residual phosphoric acid was seen being discharged from the cooling slots. This could be seen most readily in the section containing the sonic throat. The emissivity difference between the acid and background varied by as much as one order of magnitude. This resulted in a distinct infrared signature for the phosphoric acid which could be seen during successive scans. Representative images of phosphoric acid discharge are shown in figure 6. Typically, the highly-polished stainless steel walls had an emissivity from 0.05 to 0.1 while the phosphoric acid had an estimated emissivity in the range of 0.3 to 0.7.

Some of the acid which was discharged from the slots was deposited on the imager lens and scanning mirror of the infrared scanning system. Until removed, the acid deposits attenuated and scattered the infrared energy detected by the imager. The antireflection coatings on the 7 degree lens and portions of the aluminum reflective coating on one of the front surface scanning mirrors was partially destroyed as a result of the acid deposits. This acid buildup on the system optics further decreased the overall sensitivity and resolution of the scanning system.

Visual inspection of the spool piece revealed a large depression located at the approximate midpoint of the specimen and extending circumferentially around the inner wall. This visible blemish was the result of a radial slippage of a disc stack which was remachined flush with the surface. This defect was scanned with the imager in order to detect flow variations from within the newly machined area. Evidence of the scar did show up clearly in subsequent infrared images (fig. 7). In the infrared, the surface inside the flaw did not exhibit the same features as the surrounding unaffected area. There was some evidence of slot activity inside the machined area when the images were subject to image processing. Although flow was physically observed through the groove, the quality or quantity of the flow could not be determined from the infrared photographs. The surface finish in the groove did not seem to be consistent with the surrounding areas. This difference in surface finish could explain the infrared signature of the defect as detected by the imager. The emissivity of a surface is strongly dependent upon the physical characteristics of the surface. Varying the surface roughness of an object can change its emissivity by more than two orders of magnitude. (ref. 4)

During the test it became evident that the imager equipped with the 7 degree lens was unable to distinguish fine surface features and individual slots which ranged from 0.0025 to 0.008 inches in width. This lens has a rated geometrical resolution of 0.7 milliradians and a minimum focal length of 47.2 inches when operating under optimum conditions. At this distance, the lens would theoretically be able to spatially resolve separation distances only up to 0.033 inch. In addition to the resolution problem, the nozzle test section's highly-polished interior surface reflected extraneous radiation from the surroundings into the field of view of the scanner.

In order to increase the spatial resolution of the imaging system, a 25-millimeter lens extender was added to the 7 degree lens. The addition of this lens extender permitted closer focusing and brought the total optical path down to approximately 32 inches. This working distance gave a theoretical spatial resolution of approximately 0.022 inches at the rated 0.7 milliradian geometrical resolution, a 32 percent improvement which was due to the shorter overall optical pathlength.

The instanteous field of view of the imager is determined by measurement of the imagers relative response to a vertical slot, of known width, in front of a featureless warm flat plate. The manufacturers rated geometrical resolution of 0.7 milliradians is based upon the slit response of the detector at a 50 percent contrast ratio. This contrast ratio was not a suitable estimate of the bandwidth that the detector was operating at while under test conditions. The geometrical resolution observed during the survey was approximately 1.5 milliradians which would correlate to a more reasonable figure of 90 percent for the contrast ratio.

This figure for the geometrical resolution would seem to explain the nature of the images obtained from the data. Slot definition and

position were subject to great uncertainty in many of the images obtained. This would seem to indicate that the instantaneous field of view (IFOV) of the imager was greater than the target area.

As a result, the ability of the imager to detect a sampled slot with certainty would decrease since the signal received from the sampled area S consists of the signal per unit area originating from the area of the target, S_t (slot), plus the signal per unit area emitted from the background, S_b (area surrounding the slot).

$$S = (S_bA_b) + (S_tA_t)$$

Where S_b= energy per unit area emitted from background
S_t= energy per unit area emitted from target
A_b= area of background within the instantaneous field of view
A_t= area of target within the instantaneous field of view

Estimates of the Slot Area/IFOV ratio for a 0.0025-by 0.1-inch slot based on a 32-inch optical pathlength and a 1.5 milliradian geometrical resolution yield a figure of approximately 0.07. (fig. 8)

$$0.07 = A_s/IFOV$$

$$\text{Where } A_s = \text{slot area within IFOV} = (0.0025)(0.0015)(32)$$

$$IFOV = \frac{\pi}{4}[(0.0015)(32)]^2$$

A value of A_s equal to 1 indicates that the target fills the IFOV and its location and temperature could be readily detectable without additional data manipulation. A value between 0 and 1 would imply that the target area is less than the IFOV and might be detectable under some circumstances. As this ratio approaches 0, the target becomes less visible to the detector and ultimately becomes indistinguishable from the background.

In addition, the nozzle's interior surface finish permitted the observation of specular reflections throughout the inspection. Extensive shielding of the interior from external radiation sources was required to reduce the effects of reflections from within the nozzle. The high reflectivity of the nozzle's interior surface proved to be troublesome since it was possible for the region under inspection to receive and reflect radiation from other areas within the nozzle. In this environment, the radiation viewed by the imager would be comprised of the radiation emitted by the surface, plus radiation reflected by the surface but originating from an area elsewhere in the nozzle (fig. 9).

It was concluded from these results that NASA LaRC's present infrared imaging capabilities lack the required geometrical resolution to inspect the new transpiration-cooled nozzle. Although the resolving power of the current infrared imaging system was not high enough to clearly distinguish the individual slots on the interior surface, the results did show that the general technique was capable of viewing relatively large surface areas with speed and accuracy. The acquisition of an imaging system with greater resolution would permit finer surface details to be distinguished.

Attempts at interpretation of the images obtained during the survey were hampered by the effects of the highly reflective interior surface. A mathematical model of these transpiration-cooled components would be needed to develop a predictable radiometric behavior of the nozzle. This model could also assist in the interpretation of some of the misleading results. Attempts at shielding the scanned area from stray radiation from within the nozzle were not made during this inspection. Adequate shielding of the surface is expected to reduce the false images associated with the highly reflective surface. Attempts at surveying oxidized nozzle components are expected to be less successful than the inspection of new pieces. The model in Appendix D attempts to predict the results of such an undertaking.

Langley Research Center
National Aeronautics and Space Administration
Hampton, VA 23665-5225

REFERENCES

1. Holman, J. P.: "Heat Transfer," McGraw Hill Book Co., NY, 1986.

2. Barnaal, Dennis: "Digital and Microprocessor Electronics for Scientific Application," Breton Publishers, Massachusetts, 1982.

3. McWane, John W.: "Introduction to Electronics Technology," Breton Publishers, Massachusetts, 1986.

4. UNIDEX IIIa User's Manual, Ed.A-3A June 1985, AEROTECH Incorporated, 1985.

5. Thermovision 880 Operating Manual, AGEMA Infrared Systems, 1987.

APPENDIX A

AREAS RECOMMENDED FOR FURTHER STUDY BASED ON COMPOSITE IMAGES

AREA TITLE	NOZZLE SECTION	AXIAL POSITION (in)	ANGULAR POSITION (°)	COMMENTS
SPOOLB03	SPOOL	1.57	72	Acid discharge
SPOOLB05	SPOOL	1.57	120	Acid discharge
SPOOLB06	SPOOL	1.57	144	Acid discharge
SPOOLB07	SPOOL	1.57	168	Acid discharge
SPOOLB08	SPOOL	1.57	192	Acid discharge
SPOOLF01	SPOOL	7.87	24	Acid discharge
SPOOLF03	SPOOL	7.87	72	Acid discharge
SPOOLF08	SPOOL	7.87	192	Acid discharge
SPOOLF09	SPOOL	7.87	216	Acid discharge
SPOOLF10	SPOOL	7.87	240	Acid discharge
SPOOLG00	SPOOL	9.45	0	Acid discharge
SPOOLG02	SPOOL	9.45	48	Acid discharge
SPOOLG03	SPOOL	9.45	72	Acid discharge
SPOOLG05	SPOOL	9.45	120	Acid discharge
SPOOLG07	SPOOL	9.45	168	Acid discharge
SPOOLG08	SPOOL	9.45	192	Acid discharge
SPOOLG09	SPOOL	9.45	216	Acid discharge
SPOOLG10	SPOOL	9.45	240	Acid discharge
SPOOLG11	SPOOL	9.45	264	Acid discharge
SPOOLG12	SPOOL	9.45	288	Acid discharge
SPOOLG13	SPOOL	9.45	312	Acid discharge
SPOOLG14	SPOOL	9.45	336	Acid discharge
SPOOLH00	SPOOL	11.02	0	Acid discharge
SPOOLH02	SPOOL	11.02	48	Acid discharge
SPOOLH03	SPOOL	11.02	72	Acid discharge
SPOOLH04	SPOOL	11.02	96	Acid discharge
SPOOLH05	SPOOL	11.02	120	Acid discharge
SPOOLH07	SPOOL	11.02	168	Acid discharge
SPOOLH13	SPOOL	11.02	312	Acid discharge
SPOOLH14	SPOOL	11.02	336	Acid discharge
SPOOLA07	SPOOL	17.58	168	Acid discharge
SPOOLA09	SPOOL	17.58	216	Acid discharge
SPOOLA10	SPOOL	17.58	240	Acid discharge
SPOOLA11	SPOOL	17.58	264	Acid discharge
SPOOLC09	SPOOL	20.73	216	Acid discharge
SPOOLJ07	SPOOL	31.75	168	Acid discharge
SPOOLJ08	SPOOL	31.75	192	Acid discharge
STHRTA01	THROAT	30.00	36	Acid discharge
STHRTA02	THROAT	30.00	72	Acid discharge
STHRTA04	THROAT	30.00	144	Acid discharge
STHRTA06	THROAT	30.00	216	Acid discharge
STHRTA07	THROAT	30.00	252	Acid discharge
STHRTA09	THROAT	30.00	324	Acid discharge

APPENDIX A (CONTINUED)

AREAS RECOMMENDED FOR FURTHER STUDY BASED ON COMPOSITE IMAGES

AREA TITLE	NOZZLE SECTION	AXIAL POSITION (in)	ANGULAR POSITION (°)	COMMENTS
STHRTD01	THROAT	25.28	36	Acid discharge
STHRTD04	THROAT	25.28	144	Acid discharge
STHRTD05	THROAT	25.28	180	Acid discharge
STHRTD06	THROAT	25.28	216	Acid discharge
STHRTD07	THROAT	25.28	252	Acid discharge
STHRTD08	THROAT	25.28	288	Acid discharge
STHRTD10	THROAT	25.28	360	Acid discharge
STHRTE04	THROAT	23.70	144	Acid discharge
STHRTN06	THROAT	9.53	216	Acid discharge
STHRTN07	THROAT	9.53	252	Acid discharge
STHRTN08	THROAT	9.53	288	Acid discharge
STHRTN10	THROAT	9.53	360	Acid discharge
SPOOLK07	SPOOL	15.75	168	Disc Slippage
SPOOLK08	SPOOL	15.75	192	Disc Slippage
SPOOLK09	SPOOL	15.75	216	Disc Slippage
SPOOLK10	SPOOL	15.75	240	Disc Slippage
SPOOLK11	SPOOL	15.75	264	Disc Slippage
SPOOLK12	SPOOL	15.75	288	Disc Slippage

APPENDIX B

RESULTS OF FEASIBILITY STUDY

Figure 11 shows that both blocked and open slots were essentially undetectable with no air flow through them while at room temperature. Figure 12 shows that all slots were still practically undetectable with near ambient temperature air flow through them. Figures 13 and 14 show that the best open slot visibilities were obtained when air was supplied at temperatures greater than 77 °F above ambient. Although cold nitrogen gas, from evaporated liquid nitrogen, as in figure 15, produced possibly larger contrast differences between the restricted and unrestricted slots, it caused considerable frost buildup on the surface of the specimen which was undesirable. While transient temperature change conditions seemed likely to enhance the imager's capability to detect blocked slots, results of the only such test attempted, shown in figure 16, did not demonstrate even as good an ability to detect slots as the steady state method. Dry air supplied at temperatures at least 77 °F above ambient was determined to enhance slot visibility by the imager. Optimum air pressure and flow rate would have to be determined for each nozzle section during inspection.

APPENDIX C

SWITCHBOX DESIGN CONSIDERATIONS

The addressable switchbox was designed to work in conjunction with and expand the capabilities of the UNIDEX IIIa position controller. The switchbox serves as an electronically-controlled gate and is located in series with one of the outputs of the UNIDEX IIIa (fig. 4). Control over the switchbox can come from the position controller itself or by user inputs through panel mounted switches.

In order for the positioner to have control over the switchbox, it was necessary to connect the switchbox communication port to the M-output port of the UNIDEX IIIa with a 15-pin communication line.

Under certain conditions it might be necessary to manually control the positioning devices, so a provision has been made to isolate the switchbox from direct communication with the controller and have it respond to inputs from the user. This allows the user to utilize the supplied joystick to position any of the devices.

It is possible to address the M-outputs of the UNIDEX IIIa directly with the command;

M = "nnn"

A TTL signal representing "nnn" in negative logic Binary Coded Decimal (BCD) is held at the M-outputs of the UNIDEX IIIa. The switchbox was designed to alternate between one of two states corresponding to the negative logic BCD TTL signals M=001 (110) and M=002 (101) from the position controller (fig. 5). The switchbox inverts this TTL signal into positive logic and then utilizes it to trigger a J-K FLIP FLOP. The output of the J-K FLIP FLOP is then used to control a Darlington array of transistors. The transistors conduct only when M=002 appears at the inputs of the J-K FLIP FLOP. These transistors are used to operate a double throw switch through a 24-volt relay. Energizing the relay will enable the device connected to output port #2 to receive the signal from the position controller. Conversely, when the TTL signal M=001 is received, the device connected to output port #1 will receive instructions from the position controller.

APPENDIX D

EFFECTS OF WALL EMITTANCE AND BACKGROUND ON IMAGER SLOT DETECTION

When using an infrared imager as a radiometer to measure surface temperature or radiance, it is necessary to correct the data for at least the lens transmittance, atmospheric transmittance and radiance, surface emittance, and background radiation reflected off of the target. The equation used in the AGEMA TIC-8000 is a typical example of such a correction:

$$I_o=(L_o+i_o)/(t_o e_o)-(1-e_o)I_a/e_o-(1-t_o)I_{atm}/(t_o e_o)$$

$$t=EXP[-(a-b)(d_o-d_{cal})]$$

where L_o = thermal level setting
i_o = isotherm reading = IU range setting*fraction of display span
t_o = product of atmospheric transmission and system relative spectral response.
e_o = object emittance
I_a = energy emitted by surroundings
I_{atm} = energy emitted by the atmospheric path

where t = atmospheric transmission
d_o = target distance (meters)
d_{cal} = distance to calibration target during calibration (meters)
$a:b$ = calibration constants for air at specified conditions

The imager calibration relation used by AGEMA is given by the following:

$$I=R/[EXP(B/T)-F]$$

where I = imager indication (isotherm units)
T = absolute temperature
B,R,F = calibration constants

In the inspection of the 8' HTT nozzle components, the atmospheric effects were neglected because of the short optical pathlength. In the following model of the imager's response to a slot, the position weighting factor will also be neglected.

$$I_s=Kk((A_t-A_s)(e_w T_w^4+(1-e_w)FT_b^4))+KkA_s e_s T_s^4$$

where K = proportionality constant
A = target surface area
k = Stephan-Boltzman constant
T = absolute temperature
e = emittance

F = radiation shape factor between target & background
I = isotherm unit response

Subscripts:

t = total
s = slot
w = wall
b = background

Similarly, the imager response to the wall adjacent to the viewed slot, assuming uniform wall emittance distribution:

$$I_w = KA_tk(e_wT_w^4+(1-e_w)FT_b^4)$$

In order for a slot to be detectable; $:|I_s-I_w|: > I_{mrtd}$

where I_{mrtd} = blackbody minimum detectable temperature difference

Solving $:|I_s-I_w|:$ yields the following:

$$kKA_s(e_sT_s^4-e_wT_w^4-(1-e_w)FT_b^4)$$

This model shows the direct proportionality between the response difference and the viewed slot area. The response is maximized when $e_w<<e_s$, when either $F<0.1$ or $T_b<T_w$, which would have occurred during the inspection of the new components. If the components had been oxidized ($0.5 < e_w < 0.9$), when the reflections had been minimized and other variables were the same, this difference would have been much less than that of the low wall emittance case. A low value for this difference would have further reduced the probablity of detection of open slots, which is necessary for the detection of blocked ones.

If the optical resolution of the imager had been good enough such that the instantaneous field of view of the imager was less than the width of the smallest slot, then the final equation would have A_t in place of A_s, so that the same limiting case analysis is applicable.

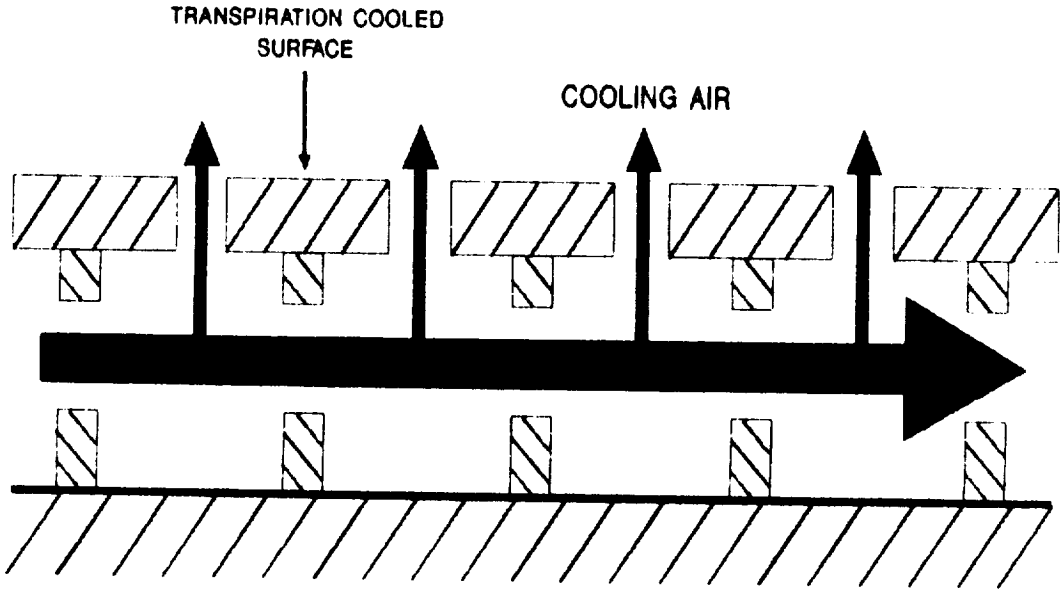

FIGURE 1. DETAILS OF A TRANSPIRATION COOLED DEVICE

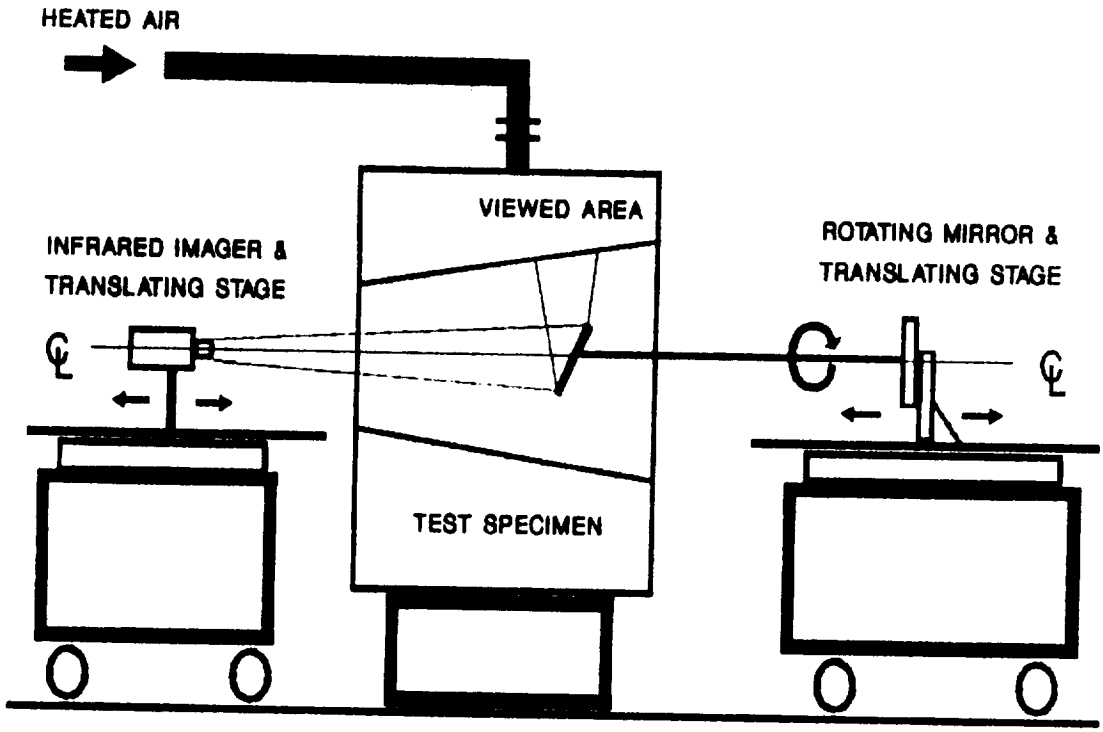

FIGURE 2. COMPONENTS UTILIZED IN A TRANSPIRATION COOLED NOZZLE INFRARED INSPECTION SYSTEM

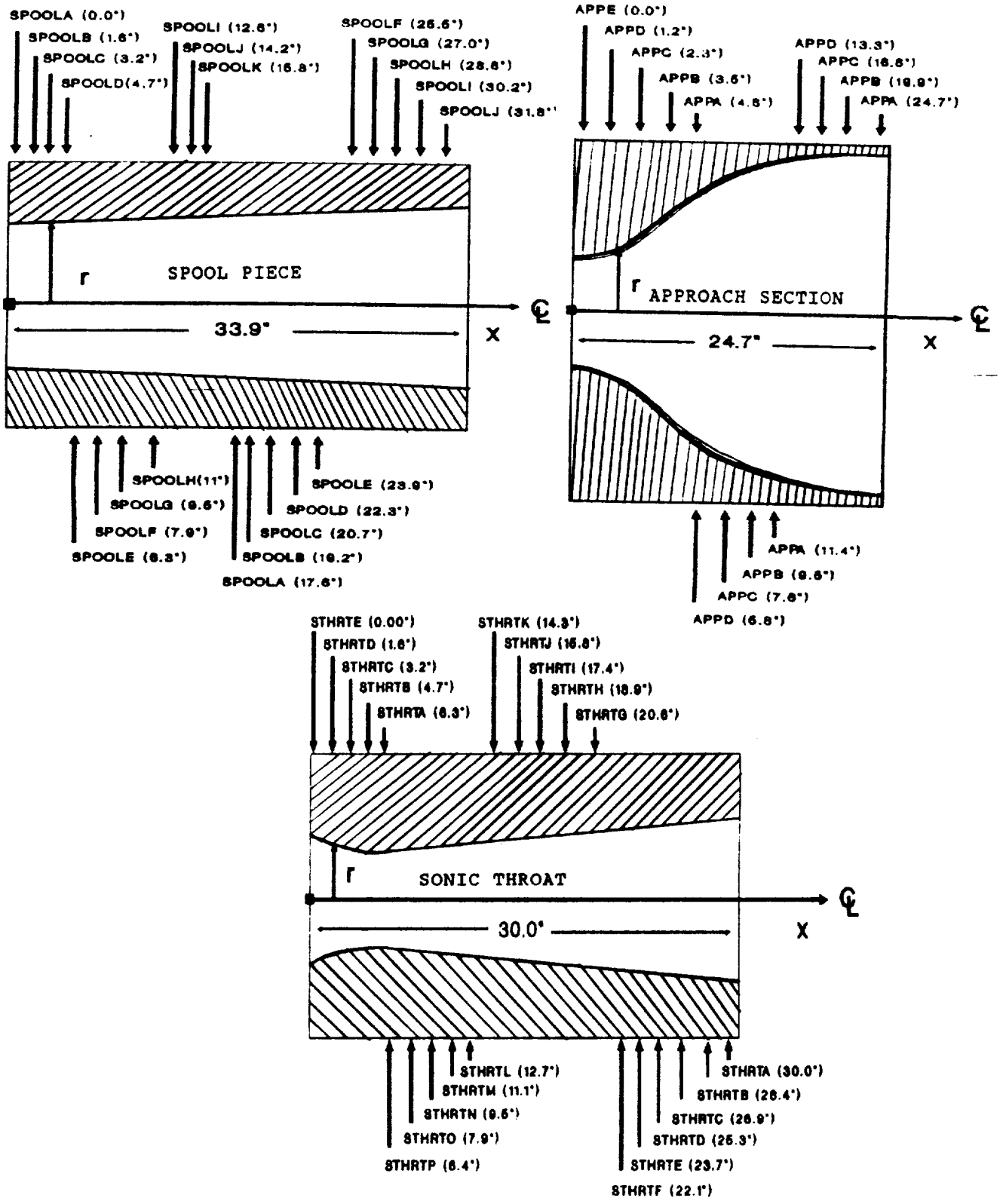

ALL DIMENSIONS IN INCHES

FIGURE 3. COORDINATE SYSTEM AND AREA TITLES FOR EACH OF THE TRANSPIRATION COOLED SUBSECTIONS

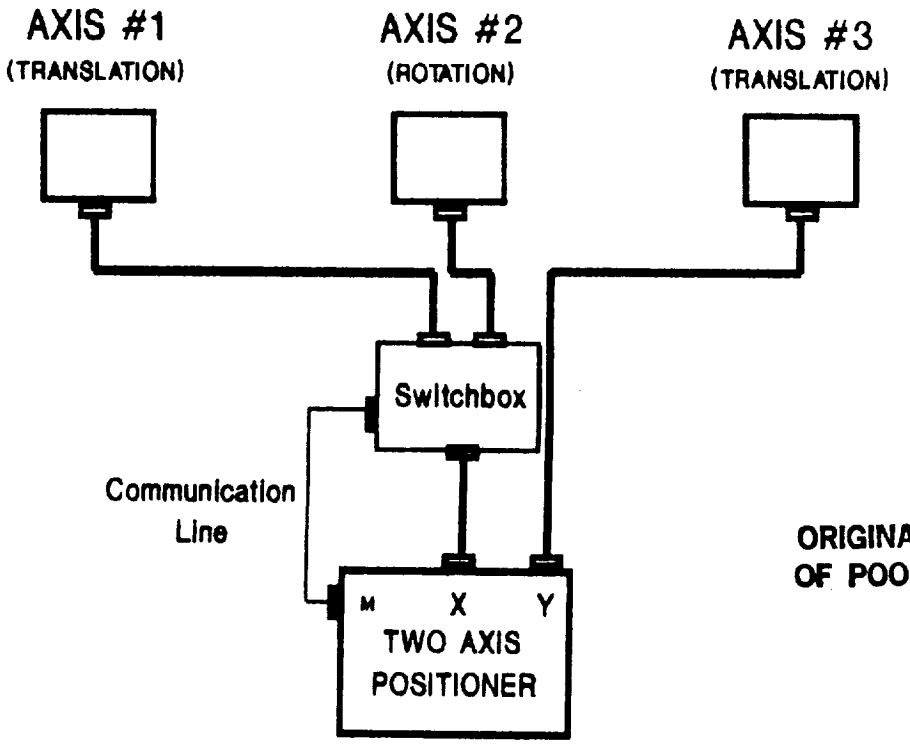

FIGURE 4. IMPLEMENTATION OF SWITCHBOX IN THE CONTROL OF THREE INDEPENDENT AXES

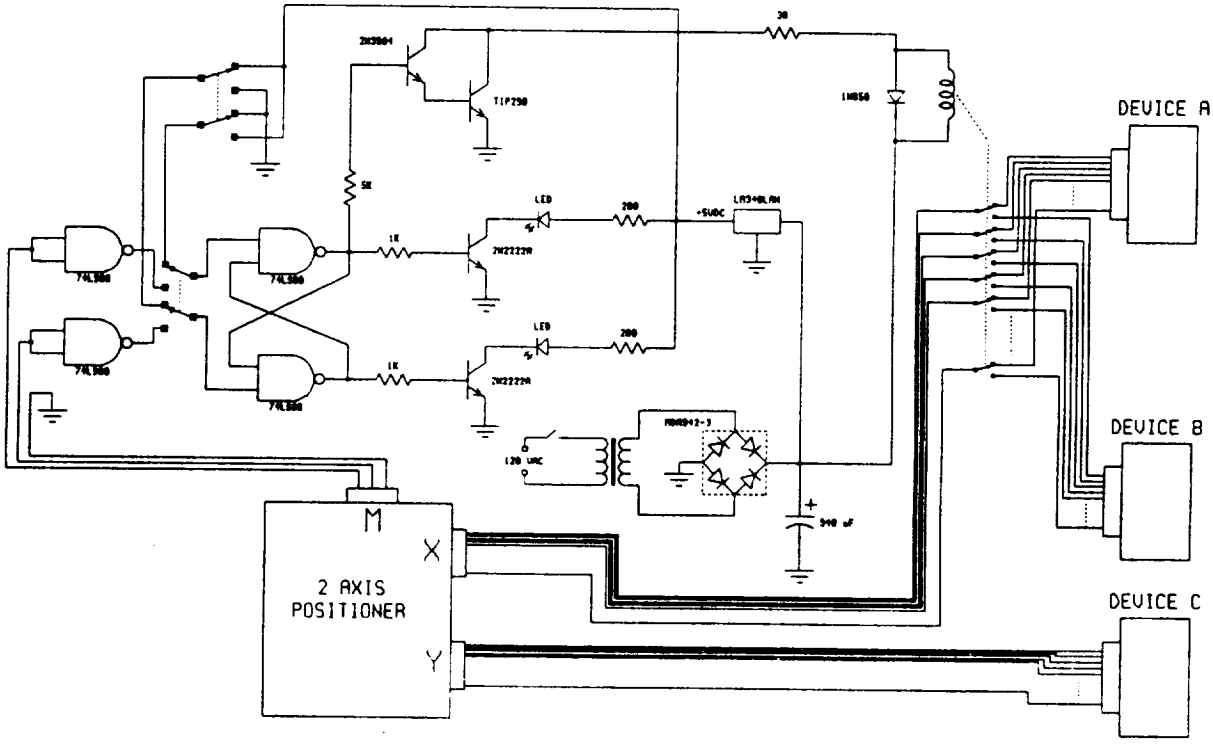

FIGURE 5. CIRCUIT DIAGRAM FOR SWITCHBOX

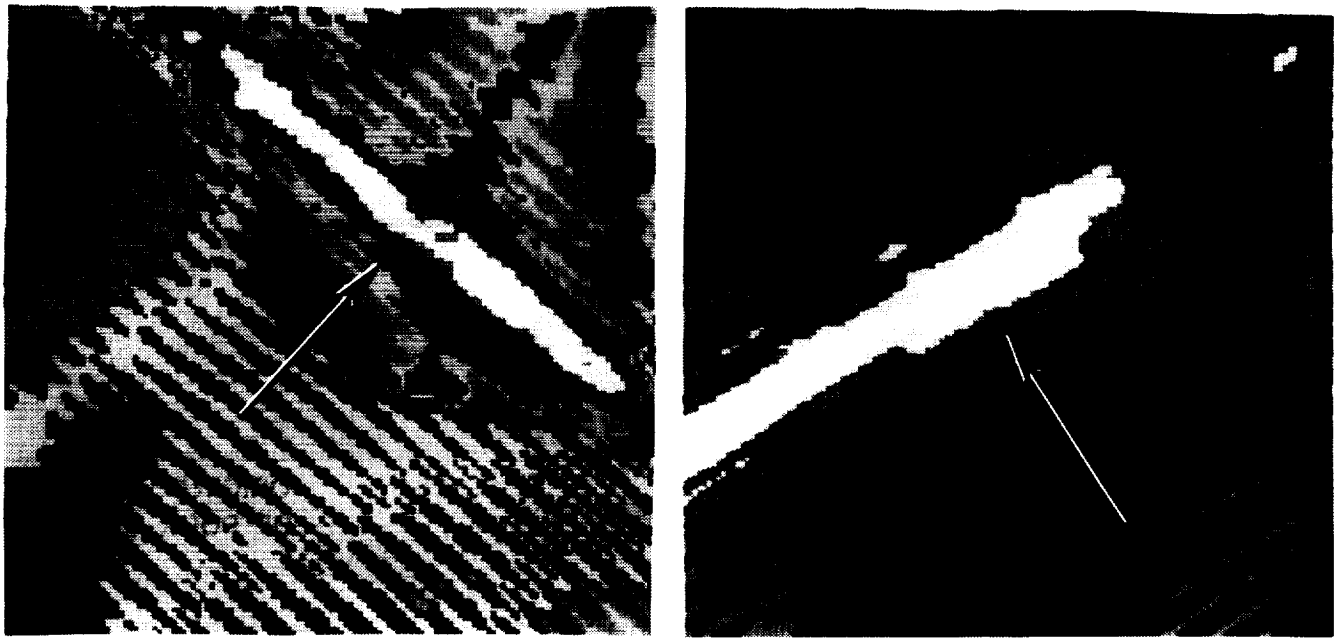

AREA TITLE: STHRTD04
LOCATION: 25.3" 144°

AREA TITLE: STHRTD06
LOCATION: 25.3" 216°

FIGURE 6. INFRARED IMAGES OF PHOSPHORIC ACID BEING DISCHARGED FROM COOLING SLOTS AT VARIOUS LOCATIONS

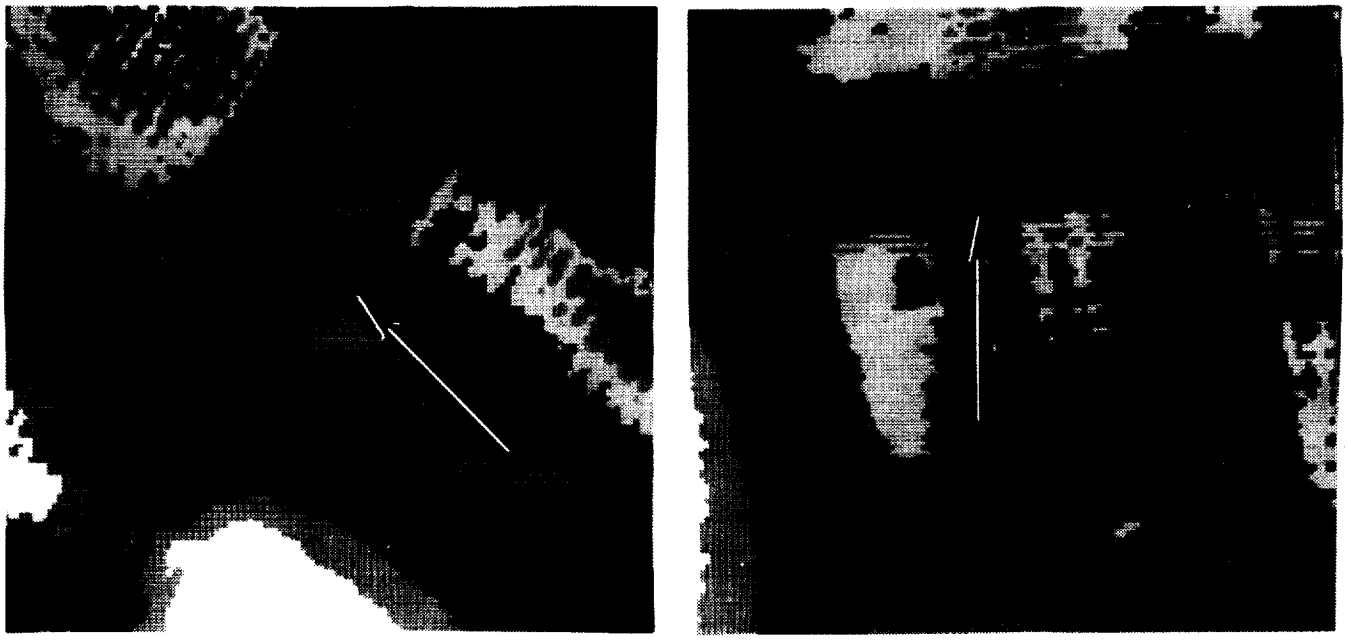

AREA TITLE: SPOOLK10
LOCATION: 15.8" 240°

AREA TITLE: SPOOLK08
LOCATION: 15.8" 192°

FIGURE 7. INFRARED IMAGES ILLUSTRATING A RADIAL DISLOCATION OF A DISC SECTION IN THE SPOOL PIECE

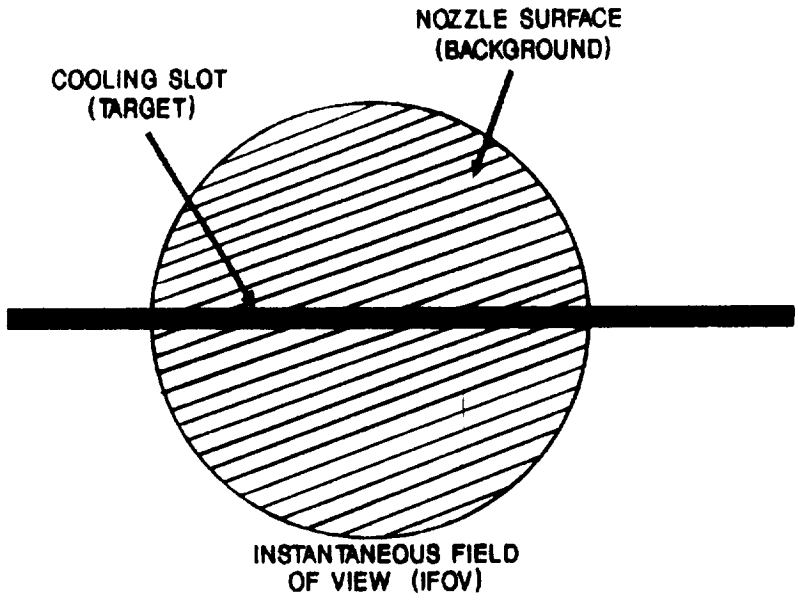

FIGURE 8. EXAMPLE OF THE SAMPLED AREA WITHIN THE IMAGER'S INSTANTANEOUS FIELD OF VIEW (IFOV).

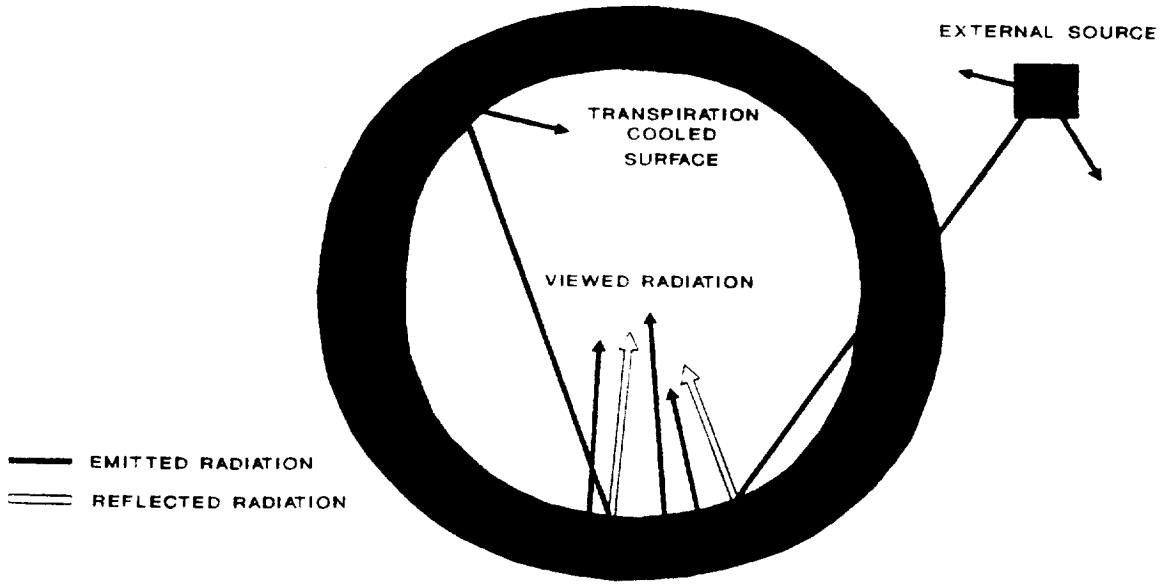

FIGURE 9. THE EFFECT OF REFLECTIONS WITHIN A PARTIALLY ENCLOSED SURFACE

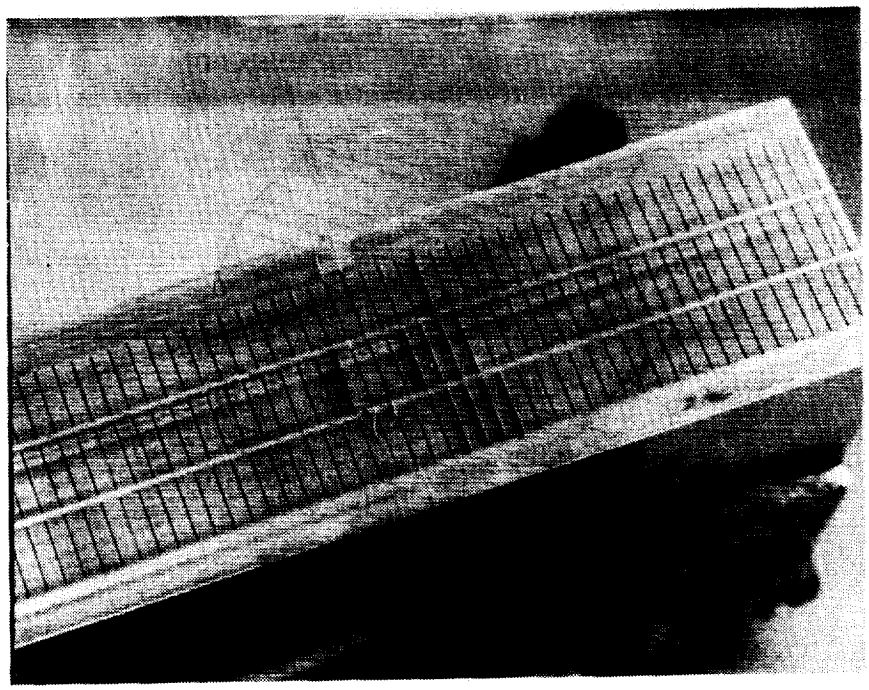

FIGURE 10. FEASIBILITY TEST MODEL WITH ARTIFICIALLY BLOCKED COOLING SLOTS

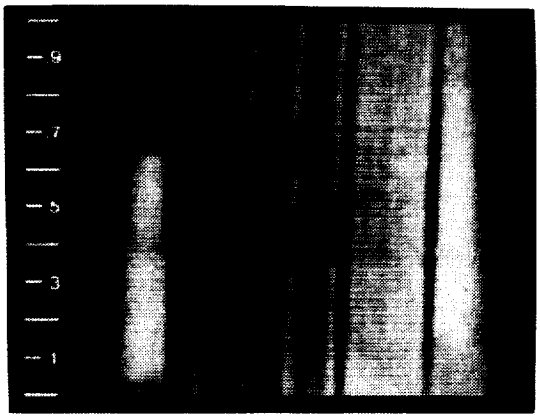

FIGURE 11.
INFRARED IMAGE OF TEST MODEL WITH NO GAS FLOW THROUGH SLOTS.

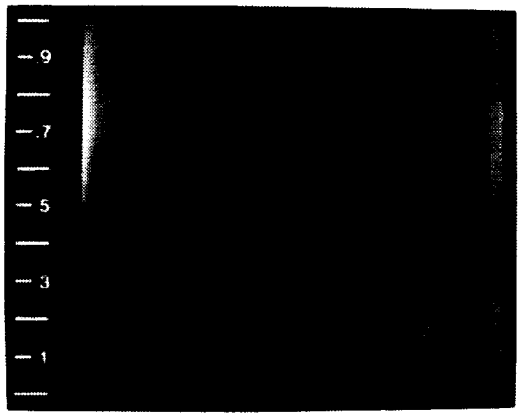

FIGURE 12.
INFRARED IMAGE OF TEST MODEL SUPPLIED WITH AMBIENT TEMPERATURE AIR.

ORIGINAL PAGE
BLACK AND WHITE PHOTOGRAPH

ORIGINAL PAGE IS
OF POOR QUALITY

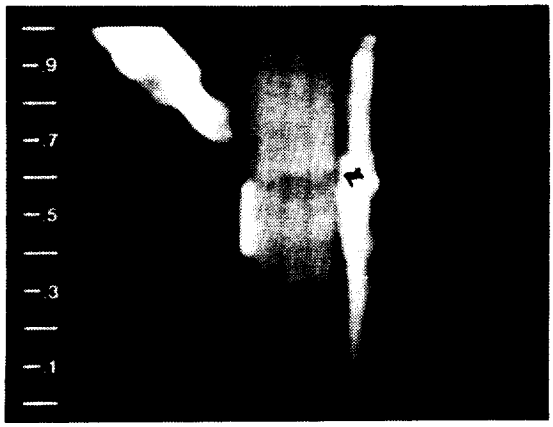

FIGURE 13.
INFRARED IMAGE OF TEST MODEL SUPPLIED WITH 150°F AIR.

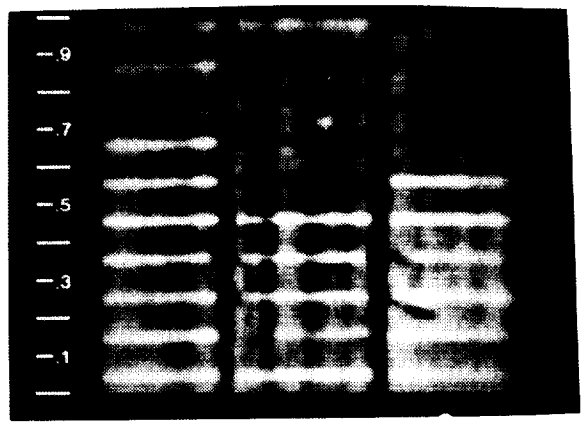

FIGURE 14.
INFRARED IMAGE OF TEST MODEL SUPPLIED WITH 150°F AIR.

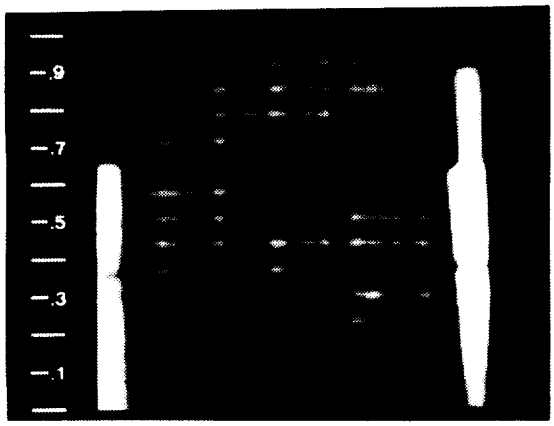

FIGURE 15.
INFRARED IMAGE OF TEST MODEL SUPPLIED WITH EVAPORATED LIQUID NITROGEN. AIR TEMPERATURE: -162°F

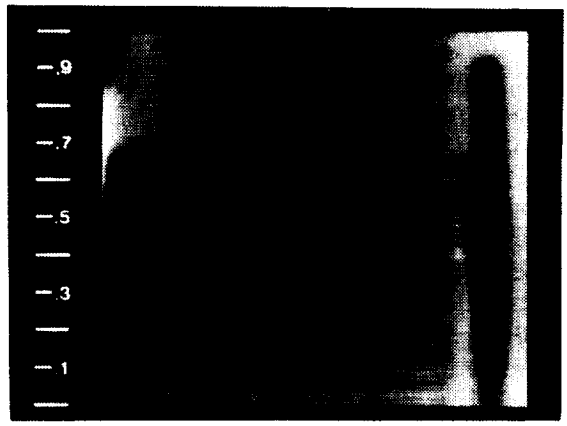

FIGURE 16.
INFRARED IMAGE ILLUSTRATING THE RESULTS OF THE TRANSIENT TEMPERATURE TEST.

NASA National Aeronautics and Space Administration

Report Documentation Page

1. Report No.	2. Government Accession No.	3. Recipient's Catalog No.
NASA TM-102608		

4. Title and Subtitle
The Utilization of an Infrared Imaging System as a Cooling Slot Blockage Detector in the Inspection of a Transpiration-Cooled Nozzle

5. Report Date
January 1990

6. Performing Organization Code

7. Author(s)
Stephen E. Borg, Robert E. Wright, Jr., David W. Alderfer and Janet Connelly Whipple

8. Performing Organization Report No.

10. Work Unit No.
505-61-01-05

9. Performing Organization Name and Address
NASA Langley Research Center
Hampton, VA 23665-5225

11. Contract or Grant No.

13. Type of Report and Period Covered
Technical Memorandum

12. Sponsoring Agency Name and Address
National Aeronautics and Space Administration
Washington, DC 20546-0001

14. Sponsoring Agency Code

15. Supplementary Notes

16. Abstract

A comprehensive examination of the 8-foot high temperature tunnel's transpiration cooled nozzle was completed using an infrared imaging radiometer to locate regions of cooling flow irregularities caused by obstruction of three or more adjacent cooling slots. Restrictions in the cooling flow were found and cataloged. Blockages found were due primarily to the presence of residual phosphoric acid being discharged from some of the cooling slots. This acid was used during construction of the nozzle components and was to have been purged prior to its delivery to the NASA Langley Research Center (LaRC). In addition, a radial displacement of one selection of discs located in the spool piece was inspected and cataloged for future reference. There did not seem to be a serious restriction of flow in this defect, but evidence from the infrared images indicated reduced slot activity within the gouge. The radiometer survey uncovered regions where closer inspection is recommended but did not cover the entire surface area of the three nozzle subsections due to equipment limitations. A list of areas with suspected problems is included in this report in Appendix A.

17. Key Words (Suggested by Author(s))	18. Distribution Statement
Infrared Imaging Temperature Measurement Transpiration Cooled Nozzle	Unclassified - Unlimited Subject Category 35

19. Security Classif. (of this report)	20. Security Classif. (of this page)	21. No. of pages	22. Price
Unclassified	Unclassified	22	A03

NASA FORM 1626 OCT 86